ASSESSING HEAT EXPOSURE RISKS AMONG DIFFERENT URBAN DEMOGRAPHICS TO ENHANCE PUBLIC HEALTH DURING HEAT WAVES

A Case Study in Nanjing

XINYUAN HAO[1], ZIYU TONG[2] and ZHICHAO YU[3]
[1,2,3] School of Architecture and Urban Planning, Nanjing University.
[1]xinyuan.hao@foxmail.com, 0000-0001-9583-6254
[2]tzy@nju.edu.cn, 0000-0002-5872-0890
[3]yzc@smail.nju.edu.cn, 0009-0000-2475-5019

Abstract. In the context of frequent extreme heat events, urban dwellers are increasingly exposed to heatwaves, leading to adverse health effects. It's crucial to precisely quantify the risk of heat exposure faced by diverse demographic groups in various locations and environments. However, current research lacked multidimensional modelling and analysis involving diverse metrics. This research quantified the risks of heat exposure by utilizing WRF-LCZ numerical simulations to obtain data during extreme heat moments. It identified areas with high heat aggregation and integrated adaptation capabilities to confront heat hazards for three groups of vulnerable populations. The research further explores variations in different heat-aggregated areas, considering diverse aspects such as built environment, social attributes, and medical support. The results indicate that: 1) Heat-aggregated areas demonstrate the highest levels of heat exposure risk during heatwave events, regardless of any other factors. 2) Specific blocks in Heat-aggregated Area 2 and 3 show significantly elevated heat exposure risks for residents under equivalent conditions, which may be influenced by poorer ventilation or higher relative humidity in the local areas. Research outputs regarding heat exposure risks can provide valuable insights for human environmental health, urban management and public facility planning.

Keywords. Heat exposure risk, Extreme heat events, Environmental health, Urban population, Weather research and forecasting (WRF), Mobile signaling.

1. Introduction

As global temperature rises, extreme weather events are becoming more and more frequent due to changing climatic environments. Among them, extreme heat events play a predominant role, increasingly impacting human society and activities, both in terms of the scale and intensity (Yin et al., 2023). Meanwhile,

the urbanization rate is expected to rise to 70% in the future, which indicates a higher urban population for residing, working and living. Therefore, it requires more scientific attention on urban built environment.

Specifically, the urban thermal environment is a significant component of the built environment in cities, affecting directly the comfort of urban residents in daily production and activities. It underscores the urgency of quantifying the heat exposure risks faced by specific populations (Han & Bu, 2023).

The heat exposure risks for different populations during extreme high-temperature weather are influenced by various factors. First, air temperature is the most immediate factor. It is clear that the heat exposure risk increases while the temperature rises in both located area and surrounding areas, implying a longer duration of sustained exposure in a high-temperature environment (Deng et al., 2023). Second, the extent of heat exposure risk during heatwaves is also influenced by the effectiveness of cooling measures adopted by individuals, the promptness of emergency services received, and the duration of these actions. The shorter time and closer proximity to emergency medical facilities help relieve from the impact of heatstroke or heat-related illnesses, while stronger treatment capabilities can alleviate symptoms and prevent multiple secondary organ failures (Choi et al., 2023). Third, the social characteristics of the population also affect their heat exposure risk and the ability to respond to heat hazards. According to *China's Expert Consensus on Heatstroke Diagnosis and Treatment (2021),* the elderly and children are most vulnerable to heat-related diseases, requiring accurate diagnosis and rapid response from medical centers. Therefore, the adaptation capacity towards heat disasters for each individual will be reduced as the density of vulnerable populations increases. To conclude, it is essential to precisely quantify the heat exposure risks regarding disparate urban populations, locations and environments, which will contribute to individual and public health.

However, previous studies remained limitations in technological pathways, analytical methodologies, dataset dimensions, and precision constrain the accuracy and validity of executing quantitative analyses of heat exposure risk in populations. Firstly, acquiring real-time data on temperature, humidity, and other weather metrics relevant to thermal comfort at specific urban locations during heatwaves poses a significant challenge (Hao & Tong, 2023). This makes comparative analyses across different instances of high temperatures less feasible (Estoque et al., 2020). Secondly, it is notably difficult to directly capture the activity characteristics of urban populations during heatwave events. Thirdly, the lack of appropriate modeling, categorization and analysis methods at the city and neighborhood scales at city and neighborhood scales complicates the risk levels of heat exposure at specific times, populations and spaces, as well as an appropriate dynamic ranking (Zhu & Yuan, 2023). Therefore, it is challenging to establish a clear linkage between urban heat risk warning information and specific moments, population characteristics and spatial scales during extreme heat events (Li et al., 2023). It is equally challenging to provide suitable mitigation recommendations for different population areas and intervention characteristics to enhance public health. This research aims to address these issues preliminarily.

2. Methodology

The study calculated the heat exposure risks by analyzing the results of WRF-LCZ simulations during extreme heat events. It identified areas with high heat exposure and evaluated adaptation strategies to mitigate heat hazards for three groups of vulnerable demographics as Figure 1 shows.
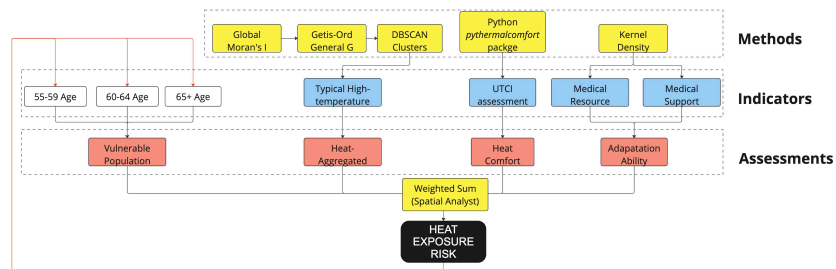
Figure 1. Methodology Framework

2.1. HEAT-AGGREGATED AREAS IDENTIFYING

We initially employed the "Global Moran's I Cluster and Outlier" method to figure out high-temperature points. This method relies on *Tobler's First Law of Geography,* which states that everything is related to everything else, but near things are more related than distant things. Thus, "spatial autocorrelation coefficient", measured by the Global Moran's I method, considers the positions and attribute values of specific features. For this analysis, we utilized data of urban surface temperatures at 12 p.m. during typical heat events, derived from WRF-LCZ numerical simulations. These data served as the features, with the numerical values (TSK variable) at each grid point considered as feature attributes, and the grid point's locations as feature positions. Then we calculated the global spatial autocorrelation coefficient in the study area to identify high-temperature points. This statistical process was conducted in ArcGIS Pro 3, with the following formula:

$$I = \frac{n}{S_0} \frac{\sum_{i=1}^{n} \sum_{j=1}^{n} w_{i,j} z_i z_j}{\sum_{i=1}^{n} z_i^2}$$

$$S_0 = \sum_{i=1}^{n} \sum_{j=1}^{n} w_{i,j}$$

$$\mathrm{E}[I] \quad = -1/(n-1)$$
$$\mathrm{V}[I] \quad = \mathrm{E}[I^2] - \mathrm{E}[I]^2$$

$$z_I = \frac{I - \mathrm{E}[I]}{\sqrt{\mathrm{V}[I]}}$$

where I represents the global spatial autocorrelation coefficient, z_i represents the deviation of the attribute of feature i from its mean $(x_i - X)$, $w_{i,j}$ represents the

spatial weight between features i and j, n represents the total number of features, and S_0 represents the aggregation of all spatial weights. I indicates stronger spatial positive correlation and clustered distributions of values when it is closer to 1.

Subsequently, we evaluated the general trends of numerical attributes within the study area with the High/Low Clustering (Getis-Ord General G) tool. This tool revealed the features of spatial clustering and identified the surrounding relationships. To be specific, it identified significant clusters of high temperatures (HH, high values surrounded by high values) based on the urban surface temperature values obtained from the WRF simulation results.

However, statistical errors and variations in surface heat island distributions may affect the results, as they contain noise and omit values (Wu et al., 2023). In addition, urban high-temperature areas, influenced by heat transfer between land parcels, should exhibit several relatively concentrated clusters. Therefore, we statistically figured out clusters with similar high-temperature phenomena by using a density-based clustering algorithm (DBSCAN). This statistical analysis was conducted using ArcGIS Pro 3, utilizing the high-temperature points clustered from the previous steps and employing flexible distance to separate clusters of different densities from sparse noise points. This statistical process outputs urban heat-aggregated areas based on high-temperature positions and values within the study area.

2.2. HEAT COMFORT CALCULATION BY UTCI

We assessed residents' thermal comfort by calculating the Universal Thermal Climate Index (UTCI) during extreme heat events. This is a widely used quantitative indicator that takes into account physiological effects in hot environments. The UTCI value is calculated by the air temperature (°C), surface wind speed at 10 meters (m/s), relative humidity (%), and mean radiant temperature (°C). The first three metrics can be obtained from WRF-LCZ simulation results directly or indirectly. The fourth metric, mean radiant temperature, can be quantified by calculating the total amount of solar radiation absorbed, and its formula is as follows:

$$T_{mrt} = \left[\frac{R}{5.39 + 10^{-8}} + (237 + T)^4 \right]^{0.25} - 273.15$$

where T_{mrt} represents mean radiant temperature, R represents total amount of solar radiation absorbed, T represents the air temperature。
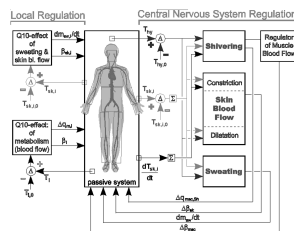
Figure 2. Heat exchange process

UTCI (°C) range	Stress Category
above +46	extreme heat stress
+38 to +46	very strong heat stress
+32 to +38	strong heat stress
+26 to +32	moderate heat stress
+9 to +26	no thermal stress

Figure 3. UCTI classifications

Subsequently, we calculated the UTCI values by *pythermalcomfort* package, which was built following the official definition of UTCI (Deng et al., 2023). This package simulates the complicated heat exchange between human body and external weather as Figure 2 shows, then outputs the UTCI value directly. Ultimately, the UTCI calculation values can be used to evaluate the degree of human comfort stress in specific climatic environments, and the corresponding relationships are detailed in Figure 3. In summary, the statistical process produced UTCI values and assessments for urban residents in different grids, involving multiple weather and environmental metrics.

2.3. ADAPTATION CAPACITY QUANTIFYING BY ACCESSIBILITY TO MEDICAL SUPPORT

We measured the adaptation capabilities of residents located in heat-aggregated areas by quantifying the accessibility of tertiary hospital emergency centers. According to the requirements for the Diagnosis and Treatment of Heat Stroke Emergencies, the success rate and prognosis quality of heatstroke patients are directly impacted by the diverse factors, such as the time, efficiency, and accuracy of emergency diagnosis and treatment, as well as the proficiency in treating secondary symptoms. Therefore, we conducted kernel density analysis on the locations and capabilities of tertiary hospital emergency centers to map the accessibility of residents in different high-temperature areas during heat hazards.

Kernel density analysis is a non-parametric method for estimating probability density based on *Silverman's fourth-order kernel algorithm* (1986). The predicted density for each regional location (x, y) in the study area is determined by the following formula:

$$\text{Density} = \frac{1}{\left(\text{radius}^2\right)} \sum_{i=1}^{n} \left[\frac{3}{\pi} \cdot \text{pop}_i \left(1 - \left(\frac{\text{dist}_i}{\text{radius}^2} \right)^2 \right)^2 \right]$$

$$\text{For dist}_i < \text{radius}$$

where $i = 1, \ldots, \text{n}$ represents each tertiary hospital emergency center, $p_0 p_i$ represents the weight field value for point i (using bed capacity of each hospital here to measure its emergency and treatment capabilities), and dist_i represents the distance between point i and the location (x, y). The statistical output of this step described the distribution density of emergency centers regarding their locations and treatment capacities.

2.4. HEAT EXPOSURE RISK CALCULATION

We proposed the concept of "Heat Exposure Risk Index (HER)" to quantify the risk for specific populations in heat-aggregated areas at designated moments during heat exposure events. We utilized a Weighted Sum (Spatial Analyst) method to establish a multidimensional model that integrates key factors, including moment, region, population, and adaptation capabilities, to conduct the calculation. Firstly, we acquired the legitimate and anonymous mobile signal data from telecommunications operators, filtered out the demographic information of three vulnerable age groups: 55-59, 60-64, 65 and above (Zhu & Yuan, 2023) in

the heat-aggregated areas. Secondly, we calculated the population density of identified groups within each grid (150m*150m region). Finally, we developed the weighted sum model to calculate the individual heat exposure risk values for each age group within specific heat-aggregated areas. The model is based on the results of thermal comfort and adaptation capabilities. The formula is as follows,

$$\text{HER}_i = \frac{r \cdot w_{ij1} \cdot S_i \cdot w_{ij2} \cdot Z_i}{w_{ij3} \sum_{ij}^{M}}$$

where HER_i represents the heat exposure risk value at location i during the extreme hot moment, w_{ij} represents the spatial weight between locations i and j, r represents the risk coefficient for different age groups, Z_i represents the population density for a specific age group at location i, S_i represents the thermal comfort assessment at location i, $\sum_{ij}^{M}$ indicates the sum adaptation capacity.

3. Case Study

The main urban area of Nanjing was chosen as the study area for its typical extremely hot summers, urbanized development and high population density. Nanjing is located north of 30°N latitude and has a subtropical monsoon climate, with the temperatures peaking in summers up to 40°C or more. The central six districts feature both higher building and population densities, divided into two parts by the Yangtze River to the northwest. For modeling and analysis, we chose the typical heat time on the hottest day, which was 12 p.m. on July 11, 2022 (local time).

This research utilized WRF-LCZ numerical model to simulate the weather conditions precisely in the study area at that specific moment (Figure 4). The simulation results provided various metrics for subsequent quantification and analysis as Table 1 shows.
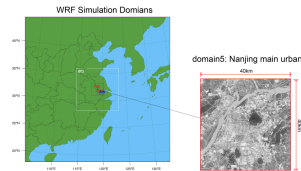
Figure 4. WRF-LCZ simulation areas

Weather Conditions	Wrfout Variables	Use
Temperature (ground surface skin)	TSK	Identifying Heat Areas / Calculating UTCI
Wind speed at 10m	U10, V10	Calculating Wind Speed for UTCI
Pressure	PSFC, P	Calculating Relative Humidity for UTCI
Water vapor mixing ratio	QVAPOR	Calculating Relative Humidity for UTCI

Table 1. Wrfout varaibles for analysis

4. Results

4.1. HEAT-AGGREGATED AREAS MAPPING
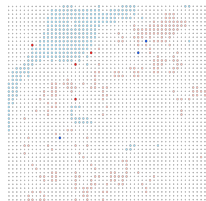
Figure 5. Temperature clusters

Figure 6. 8 Heat-Aggregated Areas

We first identified clusters of high-temperature points (Figure 5) via temperature data obtained through numerical simulations. Then we extracted the grid points encompassed and utilized the DBSCAN statistical method to identify clusters of high-temperature aggregation, representing regions with more pronounced clustering characteristics. In addition, we categorized them into 8 Heat-Aggregated Areas based on geographical distance and the characteristics of high-temperature clusters (Figure 6).

4.2. HEAT COMFORT MAPPING

We input the metrics of air temperature (˚C), wind speed at 10 meters (m/s), relative humidity (%), and mean radiant temperature (˚C) to Python to generate UTCI values for all grids in the study area. From this dataset, we extracted UTCI values and distribution for the previously identified 8 Heat-Aggregated Areas. The results reveal extensive "very strong heat stress" in most urban areas of Nanjing City during heatwaves, while "extreme heat stress" in Heat-Aggregated Areas with UTCI values above 48 ((Figure 7).
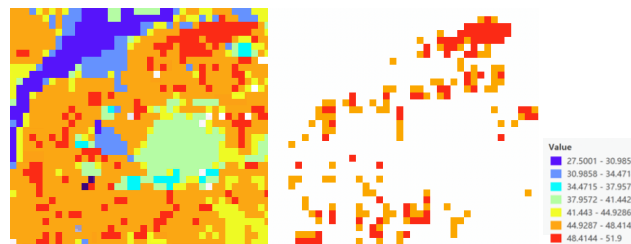
Figure 7. UTCI distributions

4.3. ADAPTATION CAPACITY MAPPING

Taking the coordinates of tertiary hospitals' outpatient departments and numbers of beds to quantify their emergency adaptation capacity during extreme heat events, we generated a density map of medical emergency services in the central urban area (Figure 8). The results described the distribution of medical support in the main urban area of Nanjing, particularly indicating stronger capability in the central six districts (primarily located within Heat-Aggregated Areas labeled as No. 4, 5, and 6 in this study). The accessibility decreased as the distance from these central areas increased.
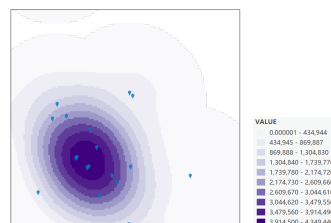
Figure 8. Accessibility to tertiary hospitals' outpatient departments

4.4. VULNERABLE DEMOGRAPHIC DENSITY MAPPING

We mapped the population distribution at specific moments by leveraging mobile signal data provided by telecommunication carriers. In this study, we primarily utilized age-classification fields to analyze the locations and population density of vulnerable groups during the heatwave event as Figure 9 shows. The figure illustrated the distribution density of three age groups (55-59 years old, 60-64 years old, 65 years old and above) at noon on July 11, 2022. It is evident that the elderly population density in the central and western regions (labeled as No. 4, 5, and 6 Heat-Aggregated Areas) is higher than that in the northeastern regions (labeled as No. 1, 2, and 3). This discrepancy reflects that the central six districts, characterized by early urbanization, possess a higher concentration of the elderly population.
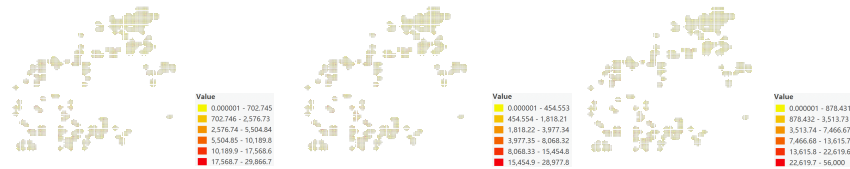
Figure 9. Density of vulnerable groups (age 55-59, age 60-64, age 65+)

4.5. HEAT EXPOSURE RISK MAPPING AND CORRELATION

We calculated heat exposure risk values and categorized the risk into 9 levels for each demographic group (see Figure 10) using the Weighted Sum (Spatial Analyst) method. The results show that the heat exposure risk values for the 55-59 and 60-64 age groups are relatively similar, while the population aged 65 and above exhibits a 300% increase in high-risk values. However, it revealed a consistent trend among different age groups after the reclassification method.
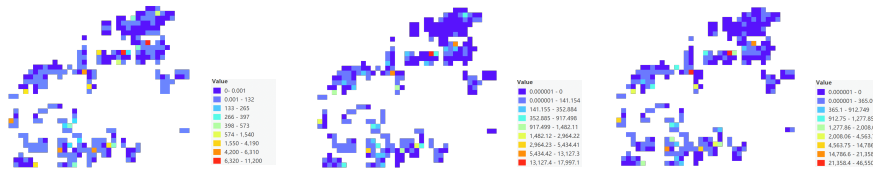
Figure 10. HER of vulnerable groups (age 55-59, age 60-64, age 65+)

Subsequently, we conducted a statistical analysis on the risk levels faced by three age groups (see Figure 11), showing that heat exposure risk was distributed similarly and UTCI values exceeded 45 consistently across the 8 Heat-Aggregated Areas. Moreover, the proportions of grids with high-risk grids (risk level=8 or 9) for all three
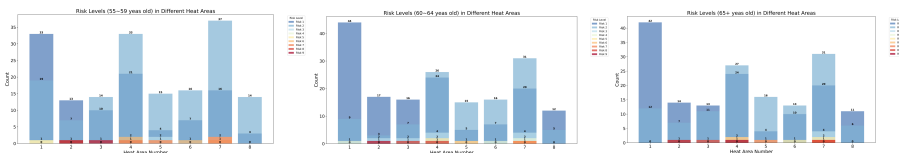
Figure 11. HER levels in 8 Heat-Aggregated Areas (age 55-59, age 60-64, age 65+)

age groups are significantly higher in the Heat-Aggregated Area 2 and 3 compared to the other areas.

5. Conclusions and Discussions

This research focuses on assessing the health of urban residents in various areas during heatwaves. It specifically emphasizes the differentiated heat exposure risk levels in different heat-aggregated areas, as exhibited by built environment characteristics and demographic features. Utilizing the numerical data at noon during the 2022 extreme heat event, we selected the main urban area of Nanjing as the study area for its high temperature, targeting the elderly population as the subject for quantifying heat exposure risks. We used various quantitative methods to conduct a multidimensional assessment of individual risk, accounting key factors such as the quality of built environment, social characteristics, and medical support.

Preliminary conclusions indicate that the overlap between high values of Universal Thermal Climate Index (UTCI) and heat-aggregated areas revealed an intensive increase in general heat exposure risks during heatwave events. In addition, the typical heat-aggregated areas exhibited the highest levels of risks, regardless of variations in geographical locations, medical resources, urban forms, and demographic characteristics. This suggests that issuing early heatwave warnings and enhancing disaster prevention knowledge are the most direct and crucial measures to reduce individual and public heat exposure risks.

On the other hand, the differentiation in heat exposure risk levels among the 8 typical heat-aggregated areas implied the inner disparate correlation between risk and temperature. It showed that the proportions of high-risk grids (risk level=8 or 9) in Heat-Aggregated Area 2 and 3 were significantly higher than in other regions. However, Area 2 and Area 3 are closely adjacent to Area 1, with similar medical accessibilities and capabilities; the residential density of the vulnerable demographics in Area 2 and Area 3 is similar to that in Area 1 as well. Therefore, it is reasonable to infer that the lower thermal comfort in certain grids led to significantly higher heat exposure risks in Area 2 and Area 3 compared to the surrounding areas. Furthermore, in the context of the similar overall temperatures in different heat-aggregated areas, the significant decrease in thermal comfort may be attributed to poor ventilation or higher relative humidity in specific blocks during heatwaves. This finding suggests effective solutions regarding other factors to lower the heat exposure risk, including urban form, architectural layouts, wind speed, and relative humidity in the built environment. Moreover, it is important to emphasize on the specific blocks and provide additional resources or support to mitigate heat exposure risks for specific demographical groups.

In conclusion, this research has revealed the various heat exposure risks faced by urban residents in different heat-aggregated areas, highlighting their variations and correlations. However, the exploration only provides a preliminary understanding. Moving forward, it's evident that there are still research gaps that need to be addressed, particularly in delving deeper into the intricacies of these risks. For example, this research focused solely on the residential population at a specific moment, excluding a comparative analysis across multiple time frames and neglecting the exploration of heat exposure risks for residents during commuting and mobility. Future research

endeavors will pursue these in-depth investigations. Furthermore, the quantification and analysis of disaster prevention capabilities could benefit from the incorporation of more refined indicators. For example, the proportion and accessibility of parks and urban green spaces may lower the risk by enhancing the urban thermal comfort. Moreover, we will adopt broader and more targeted analytical approaches to model the calculations and investigate the correlations, contributing to scientifically robust and impactful conclusions. The findings regarding heat exposure risk will provide valuable insights for human environmental health, urban management, public resource coordination, and urban planning.

References

Choi, H. M., Heo, S. & Bell, M. L. (2024). The effect modification of greenspace and impervious surface on the heat-mortality association: Differences by the dissimilarity index. *Science of The Total Environment, 908*, 168074. https://doi.org/10.1016/j.scitotenv.2023.168074

Deng, X., Cao, Q., Wang, L., Wang, W., Wang, S., Wang, S. & Wang, L. (2023). Characterizing urban densification and quantifying its effects on urban thermal environments and human thermal comfort. *Landscape and Urban Planning, 237*, 104803. https://doi.org/10.1016/j.landurbplan.2023.104803

Estoque, R. C., Ooba, M., Seposo, X. T., Togawa, T., Hijioka, Y., Takahashi, K., & Nakamura, S. (2020). Heat health risk assessment in Philippine cities using remotely sensed data and social-ecological indicators. *Nature Communications, 11(1)*, 1581. https://doi.org/10.1038/s41467-020-15218-8

Han, Y., & Bu, H. (2023). The impact of climate change on the water quality of Baiyangdian Lake (China) in the past 30 years (1991–2020). *Science of the Total Environment, 870*, 161957. https://doi.org/10.1016/j.scitotenv.2023.161957

Hao, X., & Tong, Z. (2023). Identifying the Effect of Wind Condition on Canopy Urban Heat Island: A Case Study in Nanjing. *Proceedings of the 28th Conference on Computer Aided Architectural Design Research in Asia (CAADRIA) [Volume 2]*, 623-632. https://doi.org/10.52842/conf.caadria.2023.2.623

He, L., Guo, J., Yang, W., Jiang, Q., Chen, L., & Tang, K. (2023). Multifaceted responses of vegetation to average and extreme climate change over global drylands. *Science of the Total Environment, 858(Pt 2)*, 159942. https://doi.org/10.1016/j.scitotenv.2022.159942

Li, R., Chester, M. V., Middel, A., Vanos, J. K., Hernandez-Cortes, D., Buo, I., & Hondula, D. M. (2023). Effectiveness of travel behavior and infrastructure change to mitigate heat exposure. *Frontiers in Sustainable Cities, 5*, 1129388. https://doi.org/10.3389/frsc.2023.1129388

Wu, Z., Tong, Z., Wang, M. & Long, Q. (2023). Assessing the impact of urban morphological parameters on land surface temperature in the heat aggregation areas with spatial heterogeneity: A case study of Nanjing. *Building and Environment, 235*, 110232. https://doi.org/10.1016/j.buildenv.2023.110232

Yin, J., Gentine, P., Slater, L., Gu, L., Pokhrel, Y., Hanasaki, N., Guo, S., Xiong, L. & Schlenker, W. (2023). Future socio-ecosystem productivity threatened by compound drought–heatwave events. *Nature Sustainability, 6(3)*, 259–272. https://doi.org/10.1038/s41893-022-01024-1

Zhu, W., & Yuan, C. (2023). Urban heat health risk assessment in Singapore to support resilient urban design — By integrating urban heat and the distribution of the elderly population. *Cities, 132,* 104103. https://doi.org/10.1016/j.cities.2022.104103